ATMOSPHERIC SCIENCE

Walker circulation response to extratropical radiative forcing

Sarah M. Kang[1]*, Shang-Ping Xie[2], Yechul Shin[1], Hanjun Kim[1], Yen-Ting Hwang[3], Malte F. Stuecker[4], Baoqiang Xiang[5,6], Matt Hawcroft[7,8]

Walker circulation variability and associated zonal shifts in the heating of the tropical atmosphere have far-reaching global impacts well into high latitudes. Yet the reversed high latitude–to–Walker circulation teleconnection is not fully understood. Here, we reveal the dynamical pathways of this teleconnection across different components of the climate system using a hierarchy of climate model simulations. In the fully coupled system with ocean circulation adjustments, the Walker circulation strengthens in response to extratropical radiative cooling of either hemisphere, associated with the upwelling of colder subsurface water in the eastern equatorial Pacific. By contrast, in the absence of ocean circulation adjustments, the Walker circulation response is sensitive to the forcing hemisphere, due to the blocking effect of the northward-displaced climatological intertropical convergence zone and shortwave cloud radiative effects. Our study implies that energy biases in the extratropics can cause pronounced changes of tropical climate patterns.

INTRODUCTION

The Walker circulation is a key element of tropical climate, with air rising in the western equatorial Pacific and descending in the eastern equatorial Pacific. The Walker circulation strength is tightly coupled to the east-west contrast in equatorial Pacific sea surface temperature (SST) (*1*–*3*) through Bjerknes feedback (*4*). While tropical ocean-atmosphere interactions have been emphasized in the literature, recent studies hint at an extratropical impact on the equatorial Pacific SST and hence the Walker circulation. For instance, a prescribed radiative heating over the Southern Ocean (50°S to 80°S) is shown to reduce the zonal SST gradient in the equatorial Pacific (*5*), while a prescribed radiative cooling between 30°S and 60°S increases this gradient (*6*). Moreover, the leading spatial pattern of aerosol-forced SST response during the 20th century exhibits a stronger zonal SST gradient in the equatorial Pacific (*7*). In a future warming climate, Southern Ocean heat uptake delays extratropical Southern Hemisphere (SH) warming relative to the Northern Hemisphere (NH) counterpart, which is simulated to amplify the east-west equatorial Pacific SST gradient (*8*). In addition, both Arctic and Antarctic sea ice loss in the late 21st century are projected to weaken this zonal SST contrast (*9*, *10*). Collectively, existing research highlights extratropical impacts on the spatial pattern of equatorial Pacific SST as well as its atmospheric counterpart: the tropical Walker circulation strength (*11*–*13*).

An oceanic pathway for the extratropics–to–Walker circulation teleconnection concerns the wind-driven subtropical ocean cells that connect the subduction regions in the midlatitudes with the upwelling regions in the eastern equatorial Pacific (*14*–*17*, *10*). This suggests that extratropical cooling of either hemisphere acts to strengthen the Walker circulation, as colder water is upwelled in the eastern equatorial Pacific, strengthening the zonal equatorial SST gradient. Although this oceanic pathway is commonly invoked to explain the linkage between extratropical thermal perturbations and the Walker circulation, a possibility of the atmospheric pathway can also be found in the literature. For instance, slab ocean model (SOM) experiments reveal that the SH extratropical cooling displaces the intertropical convergence zone (ITCZ) northward, accompanying intensified southeasterly trade winds over the southeastern tropical Pacific where surface evaporation is enhanced to reduce SST (*8*, *18*, *19*). This wind-evaporation-SST (WES) feedback triggers the enhanced equatorial Pacific SST zonal contrast, which is further amplified by shortwave cloud radiative feedback, associated with changes of stratocumulus clouds in the southeastern subtropics (*6*, *8*, *19*). Conversely, an NH extratropical cooling, which leads to a southward ITCZ shift, has been shown to give rise to a reduced equatorial Pacific SST zonal contrast (*20*). Together, the Walker circulation responses to extratropical thermal perturbations seem to be dependent on the degree of atmosphere-ocean coupling (e.g., with or without ocean circulation adjustments).

Is the Walker circulation response sensitive to the hemisphere in which an extratropical energy perturbation occurs? No sensitivity is expected based on the oceanic pathway, while the atmosphere pathway would suggest a hemispheric sensitivity. The relative importance of atmospheric and oceanic pathways may vary, as extratropical energy perturbations can occur on a wide range of time scales. Our study explores the sensitivity of the Walker circulation response to the hemisphere in which an extratropical energy perturbation is imposed and the role of ocean dynamics. We perform idealized experiments in which the high latitude region of one hemisphere is radiatively cooled (fig. S1). We choose to cool, rather than to warm, the forcing region to mimic the effect of a Southern Ocean warm bias correction [i.e., climate models typically have a Southern Ocean warm bias (*21*)] and the effect of the NH extratropical aerosol forcing. To investigate the dynamical pathways in different components of the climate system, we use an atmospheric general circulation model coupled with a hierarchy of ocean models, ranging from a SOM on an idealized aquaplanet (AQUA) or a realistic continental

[1]School of Urban and Environmental Engineering, Ulsan National Institute of Science and Technology, Ulsan, South Korea. [2]Scripps Institution of Oceanography, University of California San Diego, La Jolla, CA 92093, USA. [3]Department of Atmospheric Sciences, National Taiwan University, Taipei, Taiwan. [4]Department of Oceanography and International Pacific Research Center, School of Ocean and Earth Science and Technology, University of Hawai'i at Mānoa, Honolulu, HI 96822, USA. [5]NOAA/Geophysical Fluid Dynamics Laboratory, Princeton, NJ 08540, USA. [6]University Corporation for Atmospheric Research, Boulder, CO 80301, USA. [7]University of Southern Queensland, Toowoomba, Australia. [8]Met Office, Exeter, UK.
*Corresponding author. Email: skang@unist.ac.kr

configuration to a full dynamical ocean model (DOM) (Materials and Methods). The DOM experiments are part of the Extratropical-Tropical Interaction Model Intercomparison Project (ETIN-MIP) (*22*), allowing us to examine the robustness of the DOM experiments through the analysis of nine independent fully coupled model simulations. The SOM experiments are conducted with two independent models to examine model uncertainty. Our experimental design allows us to investigate a range of physical pathways, linking the Walker circulation response to extratropical radiative forcing in the coupled climate system.

RESULTS

Role of ocean dynamics

The longitude-latitude structure of the tropical Pacific SST response exhibits marked zonal variations in both the DOM and SOM experiments (Fig. 1), despite the zonally uniform nature of the prescribed extratropical cooling forcing. In the presence of a dynamic ocean, the east-west equatorial Pacific SST gradient is enhanced in response to extratropical radiative cooling of either hemisphere (denoted as DOM-NH and DOM-SH; Fig. 1, A and B). Consequently, the Walker circulation strengthens in the DOM experiments, inferred from multiple indices from the zonal sea level pressure gradient ΔSLP (Fig. 2A; see Materials and Methods) (*23*), the surface zonal wind in the central equatorial Pacific (fig. S2A) (*24*), to the east-west contrast of the vertical velocity in the equatorial Pacific (fig. S2B) (*25*). Notably, the zonal SST contrast and associated Walker circulation responses are highly robust across the ETIN-MIP ensemble (fig. S3, A and B).

From an energetics perspective, the coupled atmosphere-ocean system responds to offset the hemispheric radiative imbalance induced by the prescribed extratropical cooling (*26*). Both the atmosphere and ocean transport energy across the equator toward the cooled hemisphere, but meridional gradients of the respective tropical response are distinct (Fig. 3A). The atmospheric energy transport response is nearly uniform in the deep tropics, associated with small horizontal gradients of the tropical free–tropospheric temperature (*27*). By contrast, the oceanic response exhibits a large divergence of energy out of the tropics as a way to transport energy into the cooled extratropics. Specifically, the divergence of energy transport response by the atmosphere is less than 40% of that by the ocean in the equatorial region (fig. S4). The extratropical oceanic energy convergence (i.e., anomalously upward net surface energy flux $Q'_{net} > 0$) in DOM-NH mostly takes place in the subpolar North Atlantic (Fig. 3C) associated with a strengthened Atlantic Meridional Overturning (fig. S5), while that in DOM-SH takes place throughout the Southern Ocean (Fig. 3D). As the ocean loses energy in the extratropics (i.e., $Q'_{net} > 0$), under the energy balance constraint, the ocean must gain energy within the tropics ($Q'_{net} < 0$) (*15*). The tropical Pacific experiences an increase of absorbed net surface energy flux, as the ocean mixed layer cools within the eastern Pacific (see the Discussion section and fig. S6) (*11*, *17*). The eastern equatorial Pacific mixed layer cooling results more from the subsurface temperature changes than from the circulation changes (fig. S7). Consistently, an energy budget analysis of the ocean mixed layer indicates that increased ocean heat uptake over the eastern Pacific is the dominant process responsible for the enhanced zonal equatorial Pacific SST contrast in the DOM experiments (T'_{OHU} in Fig. 2B; see Materials and Methods).

The effect of anomalous ocean heat uptake on enhancing the equatorial Pacific SST zonal contrast is partially cancelled by shortwave cloud radiative effects (T'_{sw} in Fig. 2B). As a result of an increased zonal asymmetry in the equatorial Pacific SST, the Walker circulation strengthens, the deep convection center over the western Pacific extends westward, and descending motion over the central and eastern Pacific intensifies (Fig. 4A). The westward shift of western Pacific deep convective activity induces a dipole structure in total cloud amount changes (Fig. 4B), leading to a negligible shortwave cloud radiative effect averaged over the western box used in the Walker circulation strength index ΔSLP (Fig. 4C). By contrast, the eastern Pacific box exhibits a substantial surface warming, as an

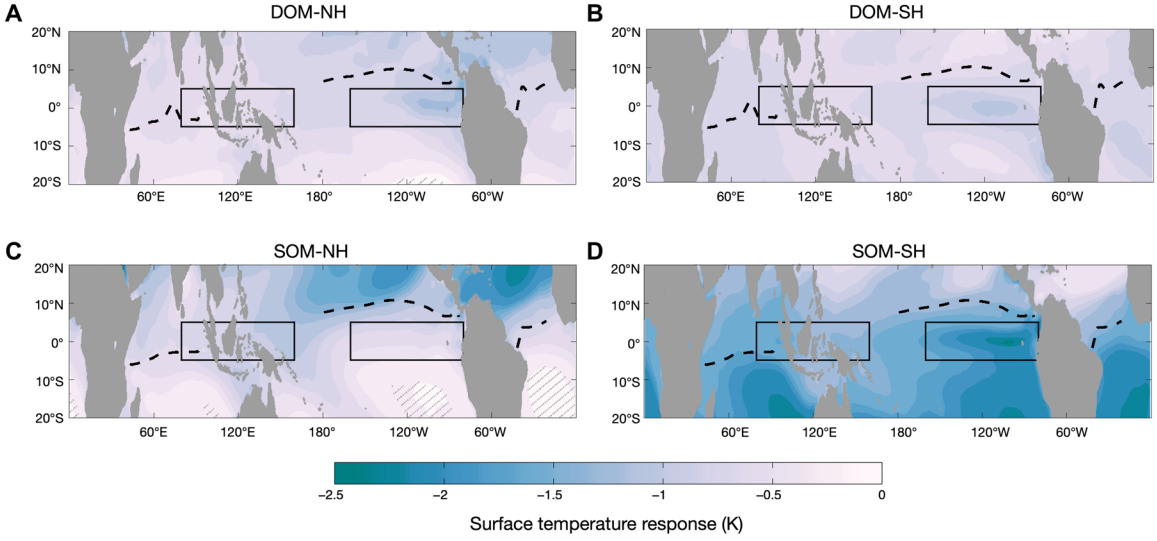

Fig. 1. Spatial pattern of the tropical climate response. Tropical SST response (shading) when (**A**) the NH extratropics or (**B**) the SH extratropics are cooled in the DOM experiments. (**C** and **D**) Same as (A) and (B) but for the SOM experiments. Hatched regions indicate statistically insignificant values at the 95% confidence level based on a two-sided *t* test. Black dashed lines indicate the climatological mean location of the ITCZ in the control experiment, defined as the latitude of maximum precipitation. Rectangles indicate the regions used to define the Walker circulation strength based on sea level pressure ΔSLP.

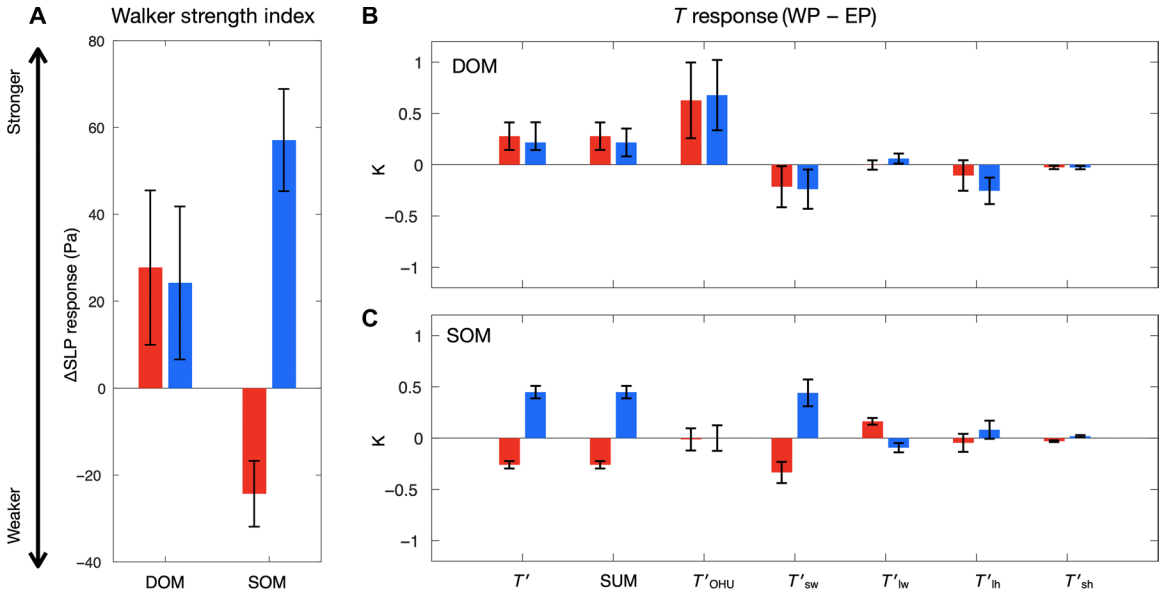

Fig. 2. The response of Walker circulation strength and zonal gradient of equatorial Pacific SST. (**A**) The Walker circulation strength index Δ*SLP* response (see Materials and Methods) in the DOM and SOM experiments. The zonal gradient of equatorial Pacific SST response and its decomposition (see Materials and Methods) in the (**B**) DOM and (**C**) SOM experiments. The red bars indicate the NH extratropics cooled case, and the blue bars indicate the SH extratropics cooled case in the GFDL model, with black error bars indicating the 95% confidence level based on a two-sided *t* test.

intensified descent over the central and eastern Pacific decreases the tropospheric relative humidity (fig. S8), leading to a total cloud amount reduction (Fig. 4B) and a more positive shortwave cloud radiative effect (Fig. 4C). As a result, the shortwave radiation changes act to partially compensate for the ocean heat uptake effect of amplifying the zonal contrast in equatorial Pacific SST (Fig. 2B). However, the effect of shortwave radiation changes on the spatial pattern of equatorial Pacific SST T'_{sw} shows a large intermodel spread with opposite signs such that the multimodel mean response is near zero (fig. S3B). Despite a considerable intermodel spread in each component of the surface energy budget, the sum of all components indicates a robust strengthening in the zonal equatorial Pacific SST contrast across all nine models (fig. S3B). It is yet to be examined whether a compensation of different surface energy components, which leads to a Walker circulation strengthening in response to extratropical cooling, is an intrinsic feature of the Earth's climate system.

Mean ITCZ blocking effect

How then does the Walker circulation respond to extratropical radiative cooling in the absence of ocean dynamical adjustment? Note that we cannot assess the transient adjustment of the forced response from the DOM experiments (including ETIN-MIP), because the effect of internal variability cannot be removed in the presence of only one long realization. To single out the responsible atmospheric dynamics, we examine the SOM experiments in which ocean dynamics is absent, while an atmosphere-ocean thermodynamic coupling exists. The SOM experiments display a distinct zonal gradient in the equatorial Pacific SST response depending on the forcing hemisphere, with a reduced gradient ("El Niño–like" pattern) for the NH extratropical cooling case (SOM-NH; Fig. 1C) and an enhanced gradient ("La Niña–like" pattern) for the SH extratropical cooling case (SOM-SH; Fig. 1D). As a result, the Walker circulation weakens in SOM-NH while it strengthens in SOM-SH (Fig. 2A).

A closer examination of the tropical SST response pattern reveals that the SOM experiments exhibit only a weak temperature response beyond the climatological ITCZ location; that is, south of the mean ITCZ position in SOM-NH and north of the mean ITCZ position in SOM-SH (Fig. 1, C and D). The northward-displaced climatological ITCZ position seems to effectively block the NH cooling from intruding toward the equator while permitting the SH cooling to penetrate across the equator through the eastern Pacific (*28*). The equatorial cooling response in SOM-NH is only 40% of that in SOM-SH (Fig. 5A), whether averaged across all longitudes or over the Pacific basin (fig. S9). An energy budget analysis of the ocean mixed layer allows us to attribute the contrast in the equatorial temperature response between the two SOM experiments primarily to changes in latent heat flux related to surface wind changes (T'_{lh} in Fig. 5B). This is because the SH extratropical cooling requires an anomalously southward cross-equatorial atmospheric energy transport (Fig. 3B), which is accomplished by a strengthening of the southern Hadley cell (fig. S10D) (*29*). As a result, the equatorial trade winds intensify (fig. S11), amplifying the equatorial SST cooling response. Conversely, the NH extratropical cooling is compensated by an anomalously northward cross-equatorial atmospheric energy transport (Fig. 3B) via a weakening of the southern Hadley cell (fig. S10C), resulting in weaker equatorial trade winds (fig. S11) and a dampened equatorial SST cooling response. Hence, the sensitivity of the equatorial temperature response to the forcing hemisphere arises, because the climatological ITCZ resides in the NH and the equator is within the southern Hadley cell.

To further confirm the blocking effect of the mean ITCZ position, we carry out idealized AQUA experiments that are designed to isolate the mean ITCZ position effect. With a hemispherically symmetric control climate (i.e., the ITCZ is located on the equator), the climate response is insensitive to the forcing hemisphere (AQUA-SYM in Fig. 5A and fig. S12A). However, under a hemispherically

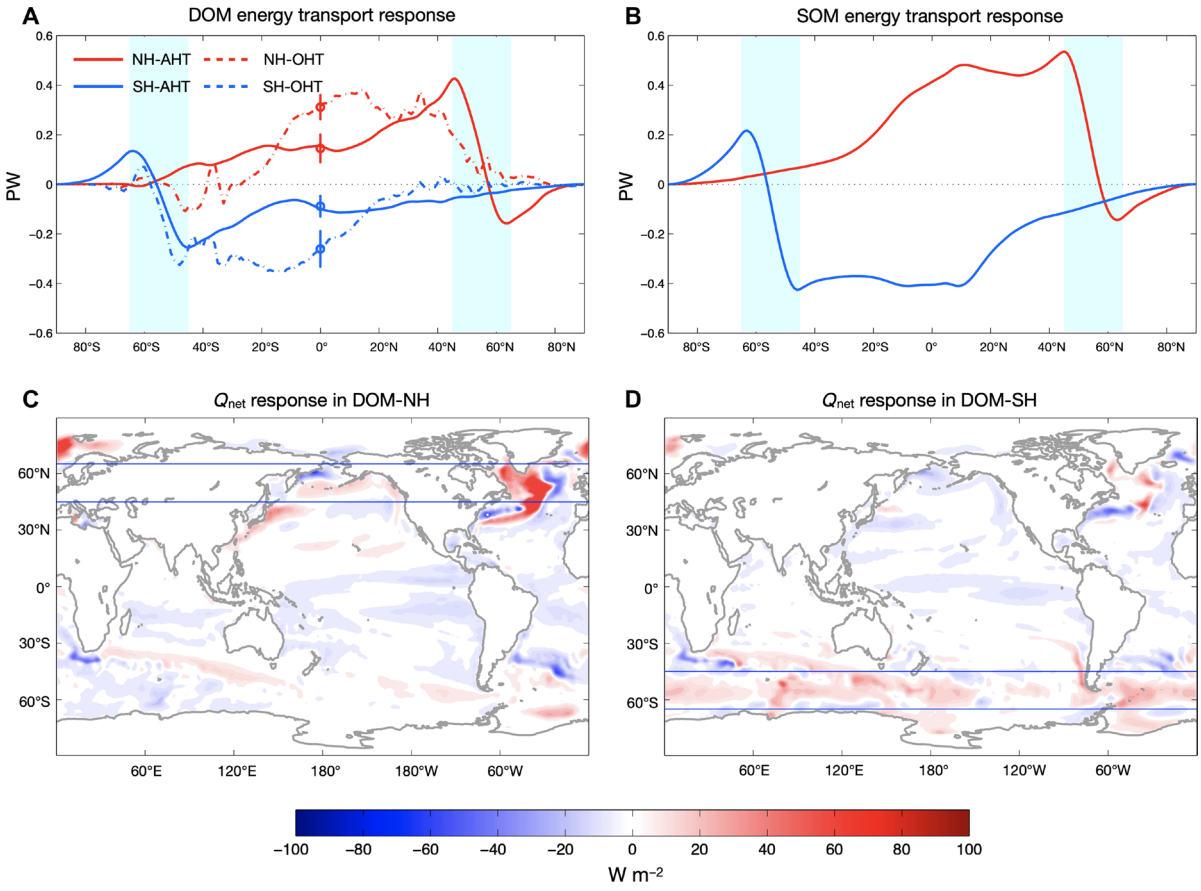

Fig. 3. The meridional energy transport and net surface energy flux responses. (**A**) The northward atmospheric heat transport (AHT; solid) and oceanic heat transport (OHT; dashed) response for DOM-NH (red) and DOM-SH (blue). The moist static energy transport for the atmosphere is indirectly computed from the net atmospheric column energy, while the oceanic energy transport indicates the Eulerian mean heat transport, which is a good approximation of the total ocean heat transport in the equatorial region. The circle symbol with an error bar indicates the ETIN-MIP multimodel mean and the model spread of equatorial values. (**B**) Same as (A) but for the SOM experiments. Blue shading in (A) and (B) indicates the forcing region. The global pattern of net surface energy flux Q_{net} response in (**C**) DOM-NH and (**D**) DOM-SH, with the forcing region indicated by blue lines. The Q_{net} response in the SOM experiments is zero by definition. Positive Q_{net} response indicates anomalously upward fluxes.

asymmetric control climate (i.e., the ITCZ is displaced northward as seen in nature), the SH perturbation produces a more pronounced equatorial temperature response than the NH perturbation (AQUA-ASYM in Fig. 5A and fig. S12B), which is consistent with our conclusions drawn from the SOM experiments. The temperature response equatorward of the forcing region declines more markedly when the climatologically warmer NH is cooled, with only a very small response equatorward of the climatological ITCZ latitude, compared to when the climatologically colder SH is cooled (fig. S12B). This hemispheric sensitivity arises in response to a prescribed warming as well (fig. S13), corroborating the ITCZ blocking effect. Hence, the AQUA experiments strongly suggest that the climatological ITCZ location acts as a barrier to the propagation of the surface temperature response. This barrier is displaced north of the equator, because the NH is warmer than the SH in the Earth's current climate (*30*).

With a realistic continental configuration, a clearly defined ITCZ is only present in the central to eastern Pacific (refer to Fig. 6, C and D); hence, the ITCZ blocking effect is also less prominent over the western Pacific. SOM-NH shows that a modest surface cooling response reaches the equatorial Pacific through the monsoon-dominated western Pacific warm pool region, slightly reducing the zonal contrast in equatorial Pacific SST (Fig. 1C). In comparison with SOM-NH, SOM-SH exhibits not only a substantially stronger equatorial cooling response (Fig. 5A) but also a reversed zonal contrast in equatorial Pacific SST response (Figs. 1, C and D, and 2C), as a result of the climatological ITCZ blocking effect.

Dependence on cloud radiative effects

The strong equatorial cooling in SOM-SH is particularly pronounced off the coast of Ecuador (Fig. 1D). The southern extratropical cooling drives anomalous meridional pressure gradients that intensify the climatological southeasterlies over the eastern basins of the subtropical South Pacific (*19*, *31*). Hence, zonal variations in climatological winds are initially responsible for shaping the spatial pattern of the equatorial Pacific cooling response through WES feedback (*8*, *19*). Consequently, the zonal contrast in the equatorial Pacific SST response excites distinct cloud feedbacks between the eastern and western basins of equatorial Pacific. The pronounced surface cooling in the eastern equatorial Pacific in SOM-SH increases the lower tropospheric stability (fig. S14), leading to more marine low clouds and an enhanced shortwave reflection (Fig. 4, B and C, and fig. S8D) (*32*). Over the western equatorial Pacific, on the other hand, convective

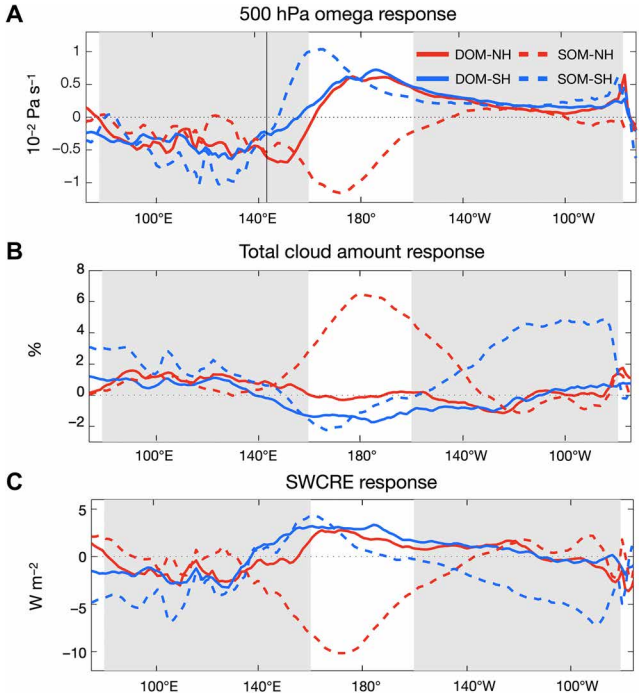

Fig. 4. Zonal variations in equatorial Pacific response. (**A**) The pressure velocity response at 500 hPa (upward in positive and downward in negative), (**B**) the total cloud amount response, and (**C**) the net shortwave cloud radiative effect (SWCRE) response over the Pacific averaged between 5°S and 5°N. Gray shaded areas indicate the regions used to define the Walker circulation strength based on sea level pressure ΔSLP. The black vertical line in (A) indicates the climatological location of maximum ascending motion in the control climate. The NH forcing case is shown in red, and the SH forcing case is shown in blue. The DOM experiments are shown in solid lines, and the SOM experiments are shown in dashed lines.

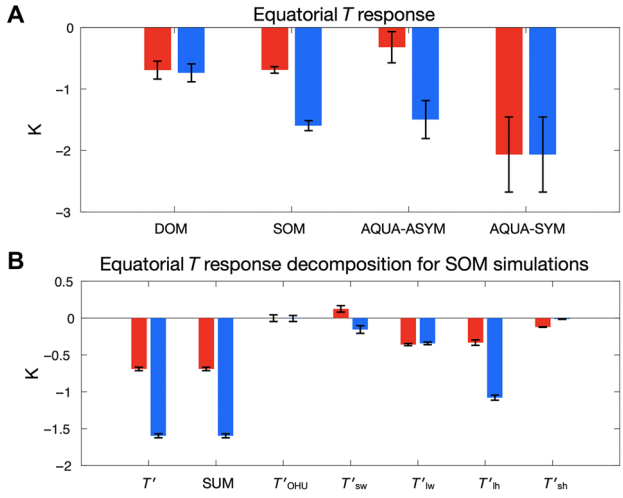

Fig. 5. Equatorial surface temperature response. (**A**) The surface temperature response averaged over 5°S to 5°N and all longitudes. (**B**) The attribution of equatorial surface temperature response in the SOM experiments (see Materials and Methods). The NH forcing case is shown in red, and the SH forcing case is shown in blue. Black error bars indicate the 95% confidence level based on a two-sided *t* test.

clouds shift westward associated with a strengthening of the Walker circulation, hence exhibiting a dipole pattern of shortwave cloud radiative forcing centered around 140°E, a location of the strongest deep convection in the control climate (Fig. 4). As a result, changes in shortwave cloud radiative effect in SOM-SH amplify the zonal contrast in equatorial Pacific SST (Fig. 2C). By contrast, with enhanced surface cooling over the western eastern equatorial Pacific in SOM-NH, the western Pacific warm pool deep convection shifts eastward, leading to a large negative shortwave cloud radiative effect in the central Pacific (Fig. 4). The resulting zonal variation of shortwave cloud radiative effects acts to reduce the zonal contrast in equatorial Pacific SST (Fig. 2C). Together, in the SOM experiments, changes in the shortwave cloud radiative effect ultimately control the sensitivity of the zonal SST gradient response to the forcing hemisphere (T'_{sw} in Fig. 2C).

Thus, in the absence of ocean dynamical adjustments, an intimate coupling between the SST spatial pattern, circulation, and cloud radiative effects manifests itself as the Walker circulation sensitivity to the hemisphere in which extratropical radiative cooling occurs. A crucial role played by clouds suggests a model dependence of the Walker circulation sensitivity due to large intermodel differences in cloud feedback (*33*). The Community Earth System Model version 1 (CESM1) exhibits a shortwave cloud radiative effect that is distinct from the Geophysical Fluid Dynamics Laboratory (GFDL) model. However, the WES feedback, with the sensitivity to the mean ITCZ position, leads to the same hemispheric sensitivity in the SST spatial pattern in the two models (fig. S3C).

DISCUSSION

It is well known that variations in the Walker circulation strength affect extratropical climate (*34*); however, a physical mechanism for the reverse pathway has not previously been scrutinized across different components of the climate system. The hierarchy of climate model experiments presented here reveals that the Walker circulation response via the atmospheric pathway is distinct, depending on in which hemisphere the extratropical forcing occurs, whereas the Walker circulation robustly strengthens in response to an extratropical cooling in either hemisphere when ocean dynamics is allowed to adjust (i.e., after the upper ocean reaches a quasi-equilibrium state) (Fig. 2A). The ETIN-MIP ensemble increases our confidence that the Walker circulation strengthening is a robust tropical response to an extratropical radiative cooling on multidecadal to centennial time scales. Consistent with previous studies (*11*, *12*), upper ocean dynamics play a major role in controlling the Walker circulation response in the fully coupled climate system: Prescribed extratropical cooling lowers the temperature of water subducted within the subtropical ocean cells, causing colder water to be upwelled in the equatorial and coastal upwelling regions, thereby strengthening the zonal SST gradient and associated Walker circulation (Fig. 6, A and B).

Our hierarchical model experiments show that the atmospheric dynamics alone causes a distinct Walker circulation sensitivity to extratropical radiative forcing. The climatologically northward-displaced Pacific ITCZ blocks the NH extratropical forcing from intruding toward the equator through the central to eastern Pacific while allowing for weak surface temperature response to reach the equator over the western Pacific where deep convection is organized around the equator. By contrast, the SH extratropical forcing preferentially perturbs the surface temperatures in the eastern equatorial

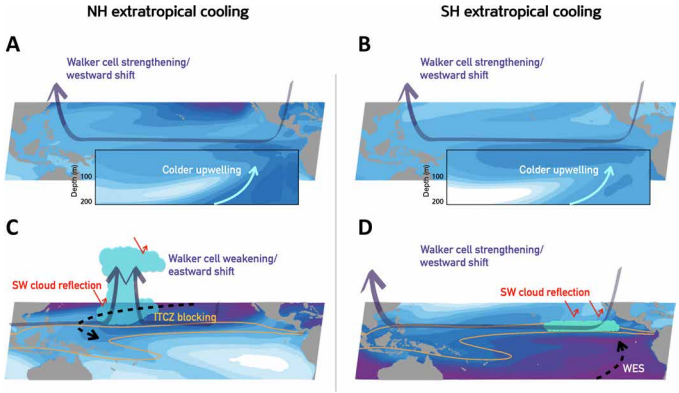

Fig. 6. Schematic summary of the physical mechanisms. (**A**) In the presence of ocean dynamics, the NH extratropical cooling induces colder subsurface water to be upwelled in the eastern equatorial Pacific, enhancing the zonal SST gradient and strengthening the Walker circulation. (**B**) Similar to (A) except for the SH forcing. (**C**) In the absence of ocean dynamics, the NH extratropical cooling affects the equatorial Pacific preferentially through the western Pacific warm pool associated with the climatological ITCZ blocking effect. The decreased zonal SST gradient is further reduced by the shortwave cloud radiative effects, weakening the Walker circulation. (**D**) Similar to (C) except for the SH forcing. The SH extratropical cooling reaches the equatorial Pacific through the eastern basin associated with climatological wind patterns via WES feedback. The increased zonal SST gradient is further enhanced by the shortwave cloud radiative effects, strengthening the Walker circulation. The horizontal map is for the SST response and the vertical cross section in (A) and (B) is for the subsurface temperature response in the equatorial Pacific. The orange contours in (C) and (D) show the 6.5 mm day^{-1} isopleth of the mean precipitation in the control experiment, denoting the climatological ITCZ location.

Pacific, because the climatological southeast trade winds allow the WES feedback from the SH. The distinct pattern of the equatorial Pacific SST response is further amplified by the shortwave cloud radiative effect, thereby creating the sensitivity of the Walker circulation response to the forcing hemisphere (Fig. 6, C and D).

One might assume that the SOM response resembles the early DOM response (say, the first few years) before the upper ocean starts adjusting to the forcing. We plan to link the SOM and DOM responses in a subsequent study by producing multiple runs with perturbed atmospheric initial conditions. Isolating the forced DOM response from the internal variability will allow us to examine the temporal evolution in the initial adjustment.

Our results suggest that extratropical climate change may be an important factor for modulating the Walker circulation. The extratropical influence may explain the recent strengthening trend of the Walker circulation in observations (*24*). For example, anthropogenic aerosols that have cooled the northern extratropics throughout the 20th century may have contributed to the observed Walker circulation strengthening. Our results imply that reducing uncertainty in simulated extratropical climate may be an important step forward for improving model simulations of tropical SST patterns and the associated Walker circulation as well as their future projections in response to radiative forcing.

MATERIALS AND METHODS

Model and experiment description

We use a developmental version of the GFDL next-generation atmospheric model version 4 (AM4) (*35*) coupled with (i) a DOM used in the GFDL Forecast-Oriented Low Ocean Resolution (*36*) under a preindustrial condition or (ii) a SOM with prescribed climatological surface heat fluxes (often referred to as Q-flux) to mimic climatological mean SSTs simulated by the DOM control experiment. Both the atmosphere and ocean models have an approximate 1° horizontal resolution. The atmospheric model has 32 vertical levels, and the ocean model has 50 vertical levels. The preindustrial control climate is perturbed by reducing solar flux over either 45°S to 65°S or 45°N to 65°N to produce a total energy perturbation of about 0.8 PW in each experiment (fig. S1). The maximum forcing magnitude of 46 W m^{-2} at 55°S/N is comparable to the intermodel spread of shortwave cloud radiative forcing over the similar latitude band in the SH (*37*). This applied radiative forcing is zonally uniform and identical except for the hemisphere that it is applied to. The NH extratropical forcing broadly corresponds to the regions of large anthropogenic aerosol emissions and/or continental ice sheets that wax and wane during glacial-interglacial cycles, while the SH forcing location corresponds to the region of pronounced cloud biases with the largest intermodel spread (*37*). These experiments can also be interpreted within the context of potential future geoengineering impacts. The DOM experiments are initialized from a fully spun-up preindustrial control run and are integrated for 150 years for both the control and perturbation experiments. The analysis is based on the average of years 101 to 150, considering that the simulations reach a quasi-equilibrium state for the upper ocean around year 70. All SOM experiments are integrated for 100 years, and the last 40 years are used for the analysis. The experiment setup in this study is the protocol used for ETIN-MIP (*22*) so that the results from nine independent fully coupled models are overlaid with the DOM experiment results in Fig. 3A and figs. S3 and S9 to confirm the robustness of the results. To address the uncertainty associated with the SOM response, the SOM experiment is also conducted with the Community Earth System Model version 1.2.2 (CESM1) (*38*), as shown in figs. S3 and S9.

In addition, the AM2 model coupled to an aquaplanet SOM (AQUA) (*39*) is used for experiments in which the degree of hemispheric asymmetry in the control climate is altered. The AQUA-ASYM experiment is forced with the zonal mean of observed surface heat flux (solid line in fig. S15) so that the NH is simulated to be warmer than the SH as in the current climate. The AQUA-SYM climate state is achieved by symmetrizing the observed surface heat flux between hemispheres (dashed line in fig. S15). The control climate with a varying degree of hemispheric asymmetry is then perturbed by adding an anomalous surface heat flux that has the same profile as the top-of-atmosphere radiative perturbations in the DOM and SOM experiments. We also examine the sensitivity to the sign of surface flux perturbations (fig. S13).

Walker circulation strength index

Following (*23*), we define the Walker circulation strength index (denoted as ΔSLP) as the sea level pressure difference over the central/east Pacific (EP; 160°W to 80°W, 5°S to 5°N) and over the Indian Ocean/west Pacific (WP; 80°E to 160°E, 5°S to 5°N; see Fig. 1). Since changes in the Walker circulation strength occur in conjunction with changes in the zonal gradient of equatorial Pacific SST, we relate ΔSLP to the surface temperature difference over the Indian Ocean/WP and over the central/EP in Fig. 2.

Surface energy budget

We diagnose the drivers of the equatorial surface temperature changes using a surface energy budget decomposition. Motivated by Hwang *et al.*

(*8*), the surface temperature response is attributed to the following factors: changes in ocean heat uptake (T'_{OHU}); changes in shortwave radiation (T'_{sw}); changes in longwave radiation (T'_{lw}); changes in latent heat flux due to variations of factors other than SST such as wind, relative humidity, or stability (T'_{lh}); and changes in sensible heat flux (T'_{sh}). Neglecting the storage term, the mixed layer energy budget in the quasi-equilibrium state can be written as

$$Q'_{\mathrm{sw}} + Q'_{\mathrm{lw}} + Q'_{\mathrm{lh}} + Q'_{\mathrm{sh}} - D'_{\mathrm{o}} = 0$$

which states that the sum of net shortwave radiation Q'_{sw}, net longwave radiation Q'_{lw}, latent heat flux Q'_{lh}, and sensible heat flux Q'_{sh} is balanced by the convergence of ocean heat transport D'_{o}. Upward fluxes are defined as positive, which heat the atmospheric column. The prime symbol indicates the difference between the two quasi-equilibrium states: the last 50-year climatology of the perturbation and the preindustrial control experiments. In the SOM experiments, D'_{o} is zero.

Following the bulk formula for evaporation, changes in the latent heat flux related with Newtonian cooling can be expressed as $Q'_{\mathrm{lh},T} = \alpha \overline{Q}_{\mathrm{lh}} T'$, where $\alpha \equiv \frac{L_{\mathrm{v}}}{R_{\mathrm{v}} \overline{T}_{\mathrm{s}}^2}$, with L_{v} being the latent heat of vaporization, R_{v} being the gas constant for moist air, T being the SST, and overbars denoting the climatology of the preindustrial experiment. The remainder, $Q'_{\mathrm{lh,others}} \equiv Q'_{\mathrm{lh}} - Q'_{\mathrm{lh},T}$, consists of latent heat flux changes due to changes in wind, changes in relative humidity, and changes in stability. Then, we have an expression for SST anomalies as

$$T' = \frac{D'_{\mathrm{o}} - Q'_{\mathrm{sw}} - Q'_{\mathrm{lw}} - Q'_{\mathrm{lh,others}} - Q'_{\mathrm{sh}}}{\alpha \overline{Q}_{\mathrm{lh}}} = T'_{\mathrm{OHU}} + T'_{\mathrm{sw}} + T'_{\mathrm{lw}} + T'_{\mathrm{lh}} + T'_{\mathrm{sh}}$$

We emphasize that T'_{lh} arises mainly through changes in surface wind. Similarity between the sum of the five terms (SUM) and the actual response (T') in Figs. 2 (B and C) and 5B verifies the applicability of the decomposition.

SUPPLEMENTARY MATERIALS

Supplementary material for this article is available at http://advances.sciencemag.org/cgi/content/full/6/47/eabd3021/DC1

REFERENCES AND NOTES

1. T. R. Knutson, S. Manabe, Time-mean response over the tropical pacific to increased CO_2 in a coupled ocean-atmosphere model. *J. Climate* **8**, 2181–2199 (1995).
2. H. Tokinaga, S.-P. Xie, C. Deser, Y. Kosaka, Y. M. Okumura, Slowdown of the Walker circulation driven by tropical Indo-Pacific warming. *Nature* **491**, 439–443 (2012).
3. S. Sandeep, F. Stordal, P. D. Sardeshmukh, G. P. Compo, Pacific Walker Circulation variability in coupled and uncoupled climate models. *Climate Dynam.* **43**, 103–117 (2014).
4. J. Bjerknes, Atmospheric teleconnections from the equatorial Pacific. *Mon. Weather Rev.* **97**, 162–172 (1969).
5. B. Xiang, M. Zhao, Y. Ming, W. Yu, S. M. Kang, Contrasting impacts of radiative forcing in the southern ocean versus southern tropics on ITCZ position and energy transport in one GFDL climate model. *J. Climate* **31**, 5609–5628 (2018).
6. C. R. Mechoso, T. Losada, S. Koseki, E. Mohino-Harris, N. Keenlyside, A. Castaño-Tierno, T. A. Myers, B. Rodrigues-Fonseca, T. Toniazzo, Can reducing the incoming energy flux over the Southern Ocean in a CGCM improve its simulation of tropical climate? *Geophys. Res. Lett.* **43**, 11,057–11,063 (2016).
7. S.-P. Xie, B. Lu, B. Xiang, Similar spatial patterns of climate responses to aerosol and greenhouse gas changes. *Nat. Geosci.* **6**, 828–832 (2013).
8. Y.-T. Hwang, S.-P. Xie, C. Deser, S. M. Kang, Connecting tropical climate change with Southern Ocean heat uptake. *Geophys. Res. Lett.* **44**, 9449–9457 (2017).
9. C. Deser, R. A. Tomas, L. Sun, The role of ocean–atmosphere coupling in the zonal-mean atmospheric response to arctic sea ice loss. *J. Climate* **28**, 2168–2186 (2015).
10. M. R. England, L. M. Polvani, L. Sun, C. Deser, Tropical climate responses to projected Arctic and Antarctic sea-ice loss. *Nat. Geosci.* **13**, 275–281 (2020).
11. N. J. Burls, A. V. Fedorov, What controls the mean east–west sea surface temperature gradient in the equatorial pacific: The role of cloud albedo. *J. Climate* **27**, 2757–2778 (2014).
12. A. V. Fedorov, N. J. Burls, K. T. Lawrence, L. C. Peterson, Tightly linked zonal and meridional sea surface temperature gradients over the past five million years. *Nat. Geosci.* **8**, 975–980 (2015).
13. Y.-C. Lin, "The fast and slow components of the tropical Pacific climate response to extratropical forcings in a fully coupled model," thesis, National Taiwan University (2020).
14. J. P. McCreary, P. Lu, Interaction between the subtropical and equatorial ocean circulations: The subtropical cell. *J. Phys. Oceanogr.* **24**, 466–497 (1994).
15. G. Boccaletti, R. C. Pacanowski, S. George, H. Philander, A. V. Fedorov, The thermal structure of the upper ocean. *J. Phys. Oceanogr.* **34**, 888–902 (2004).
16. M. F. Stuecker, A. Timmermann, F.-F. Jin, C. Proistosescu, S. M. Kang, D. Kim, K.-S. Yun, E.-S. Chung, J.-E. Chu, C. M. Bitz, K. C. Armour, M. Hayashi, Strong remote control of future equatorial warming by off-equatorial forcing. *Nat. Clim. Chang.* **10**, 124–129 (2020).
17. K. Wang, C. Deser, L. Sun, R. A. Tomas, Fast response of the tropics to an abrupt loss of arctic sea ice via ocean dynamics. *Geophys. Res. Lett.* **45**, 4264–4272 (2018).
18. S.-P. Xie, C. Deser, G. A. Vecchi, J. Ma, H. Teng, A. T. Wittenberg, Global warming pattern formation: Sea surface temperature and rainfall. *J. Climate* **23**, 966–986 (2010).
19. S. M. Kang, K. Park, Y.-T. Hwang, W.-T. Hsiao, Contrasting tropical climate response pattern to localized thermal forcing over different ocean basins. *Geophys. Res. Lett.* **45**, 12,544–12,552 (2018).
20. K. Park, S. M. Kang, D. Kim, M. F. Stuecker, F.-F. Jin, Contrasting local and remote impacts of surface heating on polar warming and amplification. *J. Climate* **31**, 3155–3166 (2018).
21. C. Wang, L. Zhang, S.-K. Lee, L. Wu, C. R. Mechoso, A global perspective on CMIP5 climate model biases. *Nat. Clim. Chang.* **4**, 201–205 (2014).
22. S. M. Kang, M. Hawcroft, B. Xiang, Y.-T. Hwang, G. Cazes, F. Codron, T. Crueger, C. Deser, Ø. Hodnebrog, H. Kim, J. Kim, Y. Kosaka, T. Losada, C. R. Mechoso, G. Myhre, Ø. Seland, B. Stevens, M. Watanabe, S. Yu, ETIN-MIP: Extratropical-tropical interaction model intercomparison project—Protocol and initial results. *Bull. Am. Meteorol. Soc.* **100**, 2589–2606 (2019).
23. G. A. Vecchi, B. J. Soden, A. T. Wittenberg, I. M. Held, A. Leetmaa, M. J. Harrison, Weakening of tropical Pacific atmospheric circulation due to anthropogenic forcing. *Nature* **441**, 73–76 (2006).
24. M. H. England, S. McGregor, P. Spence, G. A. Meehl, A. Timmermann, W. Cai, A. S. Gupta, M. J. McPhaden, A. Purich, A. Santoso, Recent intensification of wind-driven circulation in the Pacific and the ongoing warming hiatus. *Nat. Clim. Chang.* **4**, 222–227 (2014).
25. A. H. Oort, J. J. Yienger, Observed interannual variability in the hadley circulation and its connection to ENSO. *J. Climate* **9**, 2751–2767 (1996).
26. S. M. Kang, Extratropical influence on the tropical rainfall distribution. *Curr. Clim. Change Rep.* **6**, 24–36 (2020).
27. A. H. Sobel, J. Nilsson, L. M. Polvani, The weak temperature gradient approximation and balanced tropical moisture waves. *J. Atmos. Sci.* **58**, 3650–3665 (2001).
28. H. Zhang, C. Deser, A. Clement, R. Tomas, Equatorial signatures of the Pacific Meridional Modes: Dependence on mean climate state. *Geophys. Res. Lett.* **41**, 568–574 (2014).
29. S. M. Kang, I. M. Held, D. M. W. Frierson, M. Zhao, The response of the ITCZ to extratropical thermal forcing: Idealized slab-ocean experiments with a GCM. *J. Climate* **21**, 3521–3532 (2008).
30. S. M. Kang, R. Seager, D. M. W. Frierson, X. Liu, Croll revisited: Why is the northern hemisphere warmer than the southern hemisphere? *Clim. Dyn.* **44**, 1457–1472 (2015).
31. S. M. Kang, I. M. Held, S.-P. Xie, Contrasting the tropical responses to zonally asymmetric extratropical and tropical thermal forcing. *Clim. Dyn.* **42**, 2033–2043 (2014).
32. P. Ceppi, J. M. Gregory, Relationship of tropospheric stability to climate sensitivity and Earth's observed radiation budget. *Proc. Natl. Acad. Sci. U.S.A.* **114**, 13126–13131 (2017).
33. B. J. Soden, I. M. Held, An assessment of climate feedbacks in coupled ocean–atmosphere models. *J. Climate* **19**, 3354–3360 (2006).
34. N.-C. Lau, M. J. Nath, The role of the "Atmospheric Bridge" in linking tropical pacific ENSO events to extratropical SST anomalies. *J. Climate* **9**, 2036–2057 (1996).
35. M. Zhao, J.-C. Golaz, I. M. Held, H. Guo, V. Balaji, R. Benson, J.-H. Chen, X. Chen, L. J. Donner, J. P. Dunne, K. Dunne, J. Durachta, S.-M. Fan, S. M. Freidenreich, S. T. Garner, P. Ginoux, L. M. Harris, L. W. Horowitz, J. P. Krasting, A. R. Langenhorst, Z. Liang, P. Lin, S.-J. Lin, S. L. Malyshev, E. Mason, P. C. D. Milly, Y. Ming, V. Naik, F. Paulot, D. Paynter, P. Phillipps, A. Radhakrishnan, V. Ramaswamy, T. Robinson, D. Schwarzkopf, C. J. Seman, E. Shevliakova, Z. Shen, H. Shin, L. G. Silvers, J. R. Wilson, M. Winton, A. T. Wittenberg, B. Wyman, B. Xiang, The GFDL global atmosphere and land model AM4.0/LM4.0: 1. Simulation characteristics with prescribed SSTs. *J. Adv. Model. Earth Syst.* **10**, 691–734 (2018).
36. G. A. Vecchi, T. Delworth, R. Gudgel, S. Kapnick, A. Rosati, A. T. Wittenberg, F. Zeng, W. Anderson, V. Balaji, K. Dixon, L. Jia, H.-S. Kim, L. Krishnamurthy, R. Msadek, W. F. Stern, S. D. Underwood, G. Villarini, X. Yang, S. Zhang, On the seasonal forecasting of regional tropical cyclone activity. *J. Climate* **27**, 7994–8016 (2014).

37. Y.-T. Hwang, D. M. W. Frierson, Link between the double-Intertropical Convergence Zone problem and cloud biases over the Southern Ocean. *Proc. Natl. Acad. Sci. U.S.A.* **110**, 4935–4940 (2013).
38. J. W. Hurrell, M. M. Holland, P. R. Gent, S. Ghan, J. E. Kay, P. J. Kushner, J.-F. Lamarque, W. G. Large, D. Lawrence, K. Lindsay, W. H. Lipscomb, M. C. Long, N. Mahowald, D. R. Marsh, R. B. Neale, P. Rasch, S. Vavrus, M. Vertenstein, D. Bader, W. D. Collins, J. J. Hack, J. Kiehl, S. Marshall, The Community Earth System Model: A framework for collaborative research. *Bull. Am. Meteor. Soc.* **94**, 1339–1360 (2013).
39. J. L. Anderson, V. Balaji, A. J. Broccoli, W. F. Cooke, T. L. Delworth, K. W. Dixon, L. J. Donner, K. A. Dunne, S. M. Freidenreich, S. T. Garner, R. G. Gudgel, C. T. Gordon, I. M. Held, R. S. Hemler, L. W. Horowitz, S. A. Klein, T. R. Knutson, P. J. Kushner, A. R. Langenhost, N.-C. Lau, Z. Liang, S. L. Malyshev, P. C. D. Milly, M. J. Nath, J. J. Ploshay, V. Ramaswamy, M. D. Schwarzkopf, E. Shevliakova, J. J. Sirutis, B. J. Soden, W. F. Stern, L. A. Thompson, R. J. Wilson, A. T. Wittenberg, B. L. Wyman, The New GFDL Global Atmosphere and Land Model AM2–LM2: Evaluation with Prescribed SST Simulations. *J. Climate* **17**, 4641–4673 (2004).
40. D. M. W. Frierson, Y.-T. Hwang, N. S. Fučkar, R. Seager, S. M. Kang, A. Donohoe, E. A. Maroon, X. Liu, D. S. Battisti, Contribution of ocean overturning circulation to tropical rainfall peak in the Northern Hemisphere. *Nat. Geosci.* **6**, 940–944 (2013).

Acknowledgments
Funding: S.M.K., Y.S., and H.K. were supported by Basic Science Research Program through the National Research Foundation of Korea (NRF) funded by the Ministry of Science, ICT and Future Planning (2016R1A1A3A04005520 and 2017K2A9A1A06056874). S.-P.X. was supported by the National Science Foundation (AGS-1934392). Y.-T.H. was supported by the Ministry of Science and Technology of Taiwan (109-2636-M-002-011). M.H. was supported by Meat and Livestock Australia (MLA), the Queensland Government through the Drought and Climate Adaptation Program, and the University of Southern Queensland through the Northern Australia Climate Program (NACP). This is IPRC publication 1476 and SOEST contribution 11151. **Author contributions:** S.M.K. conceived the study and wrote the manuscript. S.M.K., Y.S., Y.-T.H., B.X., and M.H. designed and performed the experiments. S.M.K., S.-P.X., Y.S., and H.K. analyzed the model output and produced figures. M.F.S. assisted with framing and development of ideas. All authors contributed to the discussion of the results and the writing of the manuscript. **Competing interests:** The authors declare that they have no competing interests. **Data and materials availability:** All data needed to evaluate the conclusions in the paper are present in the paper and/or the Supplementary Materials. Additional data related to this paper may be requested from the authors.

Submitted 12 June 2020
Accepted 9 October 2020
Published 20 November 2020
10.1126/sciadv.abd3021

Citation: S. M. Kang, S.-P. Xie, Y. Shin, H. Kim, Y.-T. Hwang, M. F. Stuecker, B. Xiang, M. Hawcroft, Walker circulation response to extratropical radiative forcing. *Sci. Adv.* **6**, eabd3021 (2020).

ScienceAdvances

Walker circulation response to extratropical radiative forcing

Sarah M. Kang, Shang-Ping Xie, Yechul Shin, Hanjun Kim, Yen-Ting Hwang, Malte F. Stuecker, Baoqiang Xiang, and Matt Hawcroft

Sci. Adv., **6** (47), eabd3021.
DOI: 10.1126/sciadv.abd3021

Science Advances (ISSN 2375-2548) is published by the American Association for the Advancement of Science. 1200 New York Avenue NW, Washington, DC 20005. The title *Science Advances* is a registered trademark of AAAS.